DOI: 10.1002/ejic.200601034

Spin-Crossover Studies on a Series of 1D Chain and Dinuclear Iron(II) Triazine-Dipyridylamine Compounds

Suzanne M. Neville,[a] Ben A. Leita,[a] Daniel A. Offermann,[a] Martin B. Duriska,[a] Boujemaa Moubaraki,[a] Karena W. Chapman,[b] Gregory J. Halder,[c] and Keith S. Murray*[a]

Keywords: Iron / N ligands / Spin crossover / 1D chains / Dinuclear / Magnetic properties

Four isostructural one-dimensional polymeric iron(II) spin crossover materials containing the ligand 2-chloro-4,6-bis(dipyrid-2-ylamino)-1,3,5-triazine (cddt) have been synthesised and magnetically and structurally characterised. The polymeric material $Fe(NCS)_2(cddt)\cdot n(guest)$ (**1**), self assembles into three crystallographically distinct phases; the compounds **1b** and **1c**, $[Fe(NCS)_2(cddt)]\cdot 2(CH_3OH)$, are polymorphs, however, **1a**, $[Fe(NCS)_2(cddt)]\cdot 1/2(CHCl_3)\cdot(H_2O)$ contains a different solvent system. Each phase shows very different magnetic behaviour; phases **1a** and **1b** remain high spin over all temperatures, whilst phase **1c** undergoes a "half" spin crossover between 225 and 125 K. The structural consequences of the spin transition in **1c** have been followed using variable temperature synchrotron powder X-ray diffraction techniques. Variation of the chalcogenide ligand in the complex $[Fe(NCSe)_2(cddt)]\cdot 2(CH_3OH)$, **2**, leads to a full one-step spin crossover with a $T_{1/2}$ of 200 K. Structural analysis of **1c** below the transition temperature reveals alternating, crystallographically distinct, HS and LS iron(II) centres (HS: high spin, LS: low spin) along the chain, and structural analysis of **2** below the transition temperature reveals all LS iron(II) centres. Also reported are the structural characterisations of two dinuclear materials, containing the ligand 2,4,6-tris(dipyridin-2-ylamino)-1,3,5-triazine (tdt), of the formula $[Fe(tdt)(X)_2]_2\cdot(ClO_4)\cdot$(solvent) (X = H_2O, Cl^- for **3a**, **3b**) which are analogous to those recently reported by Gamez et al. In addition, the structural characterisations are described for dinuclear materials, containing the ligand cddt, of the formula $[Fe(cddt)(Cl)(X)]_2\cdot(Y)_2\cdot n$(solvent) (X: H_2O or $NCCH_3$, Y: ClO_4^-, BF_4^- **4a**, **4b** and **4d**) and for a cobalt(II) analogue, $[Co(cddt)(Cl)(H_2O)]_2\cdot(BF_4)_2\cdot n$(solvent) (**4c**).

Introduction

The recent papers of Gamez, Roubeau and coworkers[1,2] dealing with exchange coupling and spin crossover (SCO) in dinuclear iron(II) complexes of triazine-based bridging ligands prompts us to report our contemporaneous studies using the same ligand, and a related one. Similarities and differences in the two studies are emphasised, with a series of 1D (one-dimensional) chain SCO species being reported here for the first time. Our work forms part of a wide investigation into the synthesis, structures and magnetism of dinuclear,[3–7] and higher nuclearity,[8–14,19] iron(II) SCO compounds. We[15] and others[16] are interested in probing fundamental questions dealing with, for example, the synergy, if any, between exchange coupling and SCO, and the possible increase in cooperativity [e.g. thermal hysteresis of the spin transition(s)] in dinuclear and polynuclear SCO materials when compared to mononuclear. A range of structural designs of the bridging geometry and of the chemical nature of the bridging ligands has been employed in order to attempt to answer some of these questions.[17] The ligand common to both studies is 2,4,6-tris(dipyrid-2-ylamino)-1,3,5-triazine (labelled dpyatriz by Gamez et al.[1–2] and tdt herein, Figure 1) while the other ligand is 2-chloro-4,6-bis(dipyridin-2-ylamino)-1,3,5-triazine (labelled cddt, Figure 1).

There have been several reports recently of ligands based on dipyrid-2-ylamine (dpa) being incorporated into mono- and dinuclear systems.[1–2,4,18] The mononuclear complex $Fe(dpa)_2(NCS)_2$ containing *cis*-coordinated thiocyanate ligands, recently reported by Real et al., undergoes an incomplete one-step spin crossover with a $T_{1/2}$ of 88 K.[18] The mononuclear complex *trans*-$Fe(tdt)_2(NCS)_2$ recently reported by Gamez et al.,[2] undergoes a complete one-step spin crossover with a $T_{1/2}$ of 200 K. This was the first report for an iron(II) dpa-style material containing *trans*-thiocyanate ligands.[2] We recently reported the dinuclear complex

[a] School of Chemistry, Building 23, Monash University, Clayton, Victoria 3800, Australia
Fax: +61-3-99054597
E-mail: keith.murray@sci.monash.edu.au
[b] X-ray Science Division, Advanced Photon Source, Argonne National Laboratory, Argonne, Illinois 60439, USA
[c] School of Chemistry, University of Sydney, NSW 2006, Australia

Supporting information for this article is available on the WWW under http://www.eurjic.org or from the author.

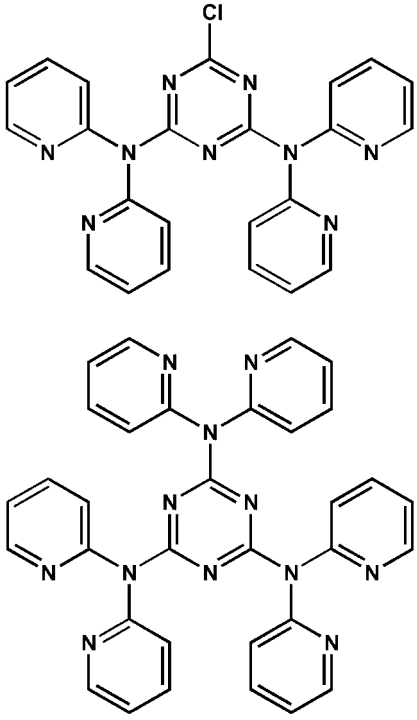

Figure 1. The ligands 2-chloro-4,6-bis(dipyrid-2-ylamino)-1,3,5-triazine (cddt) and 2,4,6-tris(dipyrid-2-ylamino)-1,3,5-triazine (tdt).

[*cis*-Fe(ddpp)$(NCS)_2$]$_2$·4(CH_2Cl_2) [ddpp = 2,5-bis(dipyrid-2-ylamino)pyridine], which undergoes a two-step spin crossover influenced by the number and type of solvent molecules present.[4] This material uniquely shows structural resolution of a "trapped" [HS-LS] state dinuclear complex (HS = high spin, LS = low spin). Here, we present a new series of 1D polymeric species containing the ligand cddt, $[Fe(NCS)_2(cddt)]\cdot 1/2(CHCl_3)\cdot(H_2O)$ (**1a**), the polymorphs $[Fe(NCS)_2(cddt)]\cdot 2(CH_3OH)$ (**1b** and **1c**) and $[Fe(NCSe)_2(cddt)]\cdot 2(CH_3OH)$ (**2**). **1c** undergoes a half spin crossover and **2** undergoes a complete spin crossover. We also report a series of dinuclear materials similar to those reported by Gamez et al.[1–2] containing the ligand tdt, $[Fe(tdt)(Cl)]_2(ClO_4)_2\cdot(C_2H_5OH)\cdot 2(CHCl_3)$ (**3a**) and $[Fe(tdt)(H_2O)]_2(ClO_4)_4\cdot 6(H_2O)$ (**3b**), and a series of dinuclear complexes containing the ligand cddt, $[Fe(cddt)(H_2O)Cl]_2(ClO_4)_2\cdot 2(C_2H_5OH)\cdot(H_2O)$ (**4a**), $[Fe(cddt)(H_2O)Cl]_2(BF_4)_2\cdot 2(C_2H_5OH)\cdot 2(H_2O)$ (**4b**), $[Co(cddt)(H_2O)Cl]_2(BF_4)_2\cdot 2(C_2H_5OH)\cdot 2(H_2O)$ (**4c**) and $[Fe(cddt)(NCCH_3)(H_2O)]_2(ClO_4)_4\cdot(NCCH_3)$ (**4d**). All attempts to incorporate the tdt ligand into polymeric iron(II) systems have thus far resulted in the formation of the monomeric spin crossover material reported by Gamez et al.[1–2]

Structural analysis on two-step/half spin crossover materials reveal that there are two ways which the octahedral environments of the iron(II) centres can be observed at the plateau temperature below the transition temperature. Firstly, it can be observed as an average Fe–N bond length between HS and LS where there is no ordering (trapping) of the LS and HS states, and secondly, as two crystallographically distinct iron(II) centres where 50% are HS and 50% LS (indeed these are the same possibilities for systems where a half spin crossover is observed). The former is by far the most commonly observed and much effort is currently being invested in understanding the two modes of crossover, in particular for dinuclear systems where two-step and half crossovers are commonly observed.[3–7] In the case of polynuclear systems, there have been relatively few examples where two-step spin crossovers are observed[8,19] and few have shown ordering of HS and LS iron(II) at the plateau region of the temperature between the two spin transitions. Here, the polymeric material $[Fe(cddt)(NCS)_2]\cdot 2(CH_3OH)$ (**1c**) undergoes a spin crossover and, at low temperatures, alternating HS and LS iron(II) centres have been observed for the first time in a 1D chain.

Initially, the present polynuclear iron(II) systems were synthesised with the intention of observing the magnetic influence of incorporating dpa style ligands into extended materials. However, the unexpected synthesis of three different crystalline phases of **1**, $[Fe(cddt)(NCS)_2]\cdot 1/2(CHCl_3)\cdot(H_2O)$ (**1a**) and $[Fe(cddt)(NCS)_2]\cdot 2(CH_3OH)$ (**1b** and **1c**), of which two are polymorphs, presents one of the first cases of polymorphism in a polymeric SCO species and as such offers a valuable opportunity to directly compare intra- and intermolecular structural effects on materials where metal centres are linked. There have been two previous reports of polymorphism in polymeric spin crossover materials, namely, $\{Fe(pmd)_2[Ag(CN)_2]_2\}$ (pmd = pyrimidine) and $\{Fe(3\text{-}CNpy)[Au(CN)_2]_2\}\cdot n(H_2O)$ (3-CNpy = 3-cyanopyridine).[20,21] The majority of reports of polymorphism have been in mononuclear iron(II) species,[22–26] in particular, the compounds [*cis*-$Fe(phen)_2(NCS)_2$][22] and [*cis*-$Fe(bipy)_2(NCS)_2$][23] (phen = 1,10-phenanthroline, bipy = 2,2-bipyridyine) exist as polymorphs and have received a large amount of interest over many years. More recently, the material $[Fe(dppa)_2(NCS)_2]$ [dppa = (3-aminopropyl)bis(pyrid-2-ylmethyl)amine] was reported[25] which forms as three crystallographically distinct polymorphs; **A**: triclinic, **B**: monoclinic and **C**: orthorhombic. The **A** phase displayed a gradual SCO, the **B** phase remained high spin and the **C** phase had an abrupt SCO with hysteresis and structurally it was tentatively explained in terms of the presence of an array of intermolecular contacts in **C** that led to more cooperativity. Guionneau et al.[26] have further investigated the structural features between two polymorphs of the compound $[Fe(PM\text{-}BiA)_2(NCS)_2]$ (PM = *N*-pyrid-2-ylmethylene and BiA = 4-aminobiphenyl) that crystallised in the same symmetry, however, they displayed gradual and abrupt spin transitions, respectively. They found a direct correlation between the abruptness of a transition and a set of structural parameters that reflected the inter- and intramolecular interactions. While it is now clearly established that intermolecular interactions, such as hydrogen bonding and π-π interactions influence spin transitions, it appears that, from one chemical example to the next, little correlation exists. Certainly, for spin crossover materials to become useful in devices, understanding the governing factors that drive cooperativity is very important. In this context, the present study compares the structural features of a series of poly-

meric spin crossover materials which reveal the presence of π-π interactions to be the primary characteristic influencing the spin transition.

Results and Discussion

Syntheses

In synthesising the 1D complexes $[Fe(NCS)_2(cddt)]\cdot n(guest)$ (**1**) [guest: $1/2(CHCl_3)(H_2O)$ for **1a**, $2(CH_3OH)$ for **1b** and **1c**] direct addition of $Fe(NCS)_2$ to cddt in the relevant solvent systems, resulted in immediate precipitation of yellow powders. In order to obtain structural information, single crystals of each phase were grown by slow diffusion techniques by using a vial for multiple solvent systems and a H-shaped tube for single solvent systems. For the materials **1b** and **1c** it was found that by using 2:4:1 ratios of Fe:NCS:cddt crystals of both phases grew together. By altering the Fe:NCS:cddt ratio to 1:2:1 it was found that that crystals of the spin crossover material **1c** could be grown with only a ca. 10% impurity of the **1b** phase. Furthermore, allowing the slow diffusion of **1c** to proceed at <5 °C the **1c** phase formed in isolation. Crystals of **1b** formed as light yellow blocks whereas crystals of **1c** formed as dark yellow-orange clumps of inter-grown crystals.

The synthesis of the dinuclear complex $[Fe(tdt)(Cl)]_2(ClO_4)_2\cdot(C_2H_5OH)\cdot 2(CHCl_3)$ (**3a**) containing the ligand tdt was carried out by slow diffusion methods in a H-tube. Single crystals of **3a** contain bound Cl^-, however, the synthesis was not carried out in the presence of chloride ions. Three possible chloride ion sources are; trace amounts from the tdt ligand synthesis, $Fe(ClO_4)_2\cdot 6(H_2O)$ and chloroform solvent. Gamez et al.[2] commented, in their synthesis of the analogous material, that the addition of stoichiometric amounts of chloride salt reduced the product yield compared to limited amounts, here whichever the chloride source is, it would be in small amounts and potentially drive the formation of the observed dinuclear. In addition, the synthesis of **3a** was carried out in the presence of $NaNCBH_3$, intended to be bound to the metal via the terminal nitrogen group, but has not been incorporated in the dinuclear material. Microanalysis of **3a** revealed a hydrated product.

The synthesis of the dinuclear complex $[Fe(tdt)(H_2O)]_2(ClO_4)_4\cdot 6(H_2O)$ (**3b**) was carried out in a mixed solvent system of methanol and acetonitrile, in air. Structural analysis revealed water molecules to be both bound to the metal, and as a solvate, and would originate from the solvent methanol and the metal salt.

The syntheses of dinuclear complexes containing the ligand cddt, $[Fe(cddt)(Cl)(X)]_2\cdot(Y)_2\cdot n(solvent)$ (X: H_2O or $NCCH_3$, Y: ClO_4^-, BF_4^- **4a**, **4b** and **4d**) and $[Co(cddt)(Cl)(H_2O)]_2\cdot(BF_4)_2\cdot n(solvent)$ (**4c**), as with **3a** did not contain any free Cl^-. The possible chloride ion sources are; trace amounts from the cddt ligand synthesis, from decomposition of the ligand and, for **4a**, from $Fe(ClO_4)_2\cdot 6(H_2O)$. While it is unclear where the chloride salt arises from it is likely from the cddt ligand. Microanalysis revealed hydrated species for each of these materials.

Magnetic Studies

The complex **1a** remains high spin over all temperatures and the $\chi_M T$ vs. temperature plot is shown in Figure S11 (see Supporting Information). The $\chi_M T$ values remain constant at 3.29 $cm^3 mol^{-1}$ K down to ca. 15 K, followed by a small decrease due to a combination of weak antiferromagnetic coupling and zero field splitting. A sufficient amount of sample of **1b** for carrying out magnetism studies was unfortunately not obtained, as it grows as an impurity in the synthesis of **1c**, and, as such, no magnetic measurements were made on this phase. However, the crystal structure of **1b** at 123(2) K revealed all iron(II) centres to be in the high spin state, and upon quench cooling of the sample in liquid nitrogen, no colour change occurred in the yellow crystals, indicating that a spin transition probably did not occur.

Plots of $\chi_M T$ vs. temperature for polycrystalline samples of **1c** and **2** are shown in Figure 2. Compound **1c** undergoes an incomplete spin crossover with what appears to be a subtle, two-step nature. At temperatures above 240 K the material is in the fully high spin state with a maximum $\chi_M T$ of 3.38 $cm^3 mol^{-1}$ K. Between 240 and 200 K there is a gradual drop in $\chi_M T$ to ca. 2.66 $cm^3 mol^{-1}$ K. Below 200 K the transition becomes even more gradual with a lowest $\chi_M T$ of 1.64 $cm^3 mol^{-1}$ K attained below 70 K, which corresponds to 50% of the iron(II) centres being in the high spin state. From 200 K to low temperatures, slow kinetics or a structural effect may prevent the completion of the spin transition.

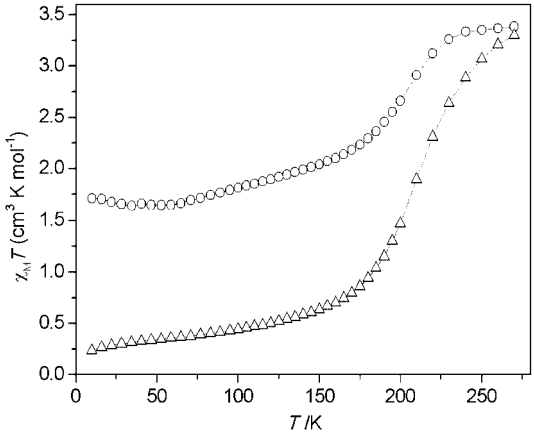

Figure 2. $\chi_M T$ vs. temperature for $[Fe(NCS)_2(cddt)]\cdot 2(CH_3OH)$ (**1c**) (o) and $[Fe(NCSe)_2(cddt)]\cdot 2(CH_3OH)$ (**2**) (Δ).

The selenocyanate analogue **2**, undergoes a full one-step spin crossover with a $T_{1/2}$ of ca. 220 K. At 270 K, a $\chi_M T$ value of 3.29 $cm^3 mol^{-1}$ K is attained corresponding to the majority of iron(II) centres being in the high spin state. The $\chi_M T$ values have not reached the LS plateau as between 270 and 170 K there is a gradual decrease in $\chi_M T$. Below 170 K

a plateau $\chi_M T$ value of 0.23 $cm^3 mol^{-1}$ K is observed corresponding to all the iron(II) centres being in the low spin t_{2g}^6 state. The non-zero magnitude of $\chi_M T$ at low temperature is a common occurrence in iron(II) spin crossover LS states and is due to second order Zeeman effects. No thermal hysteresis occurred in either **1c** or **2**.

The $T_{1/2}$ values observed for **1c** and **2** are similar in size to that observed by Gamez et al.[1,2] for Fe(dpyatriz)$_2$(NCS)$_2$, ca. 200 K. Each of these materials contains the *trans*-Fe(DPA)$_2$(NCS)$_2$ coordination environment and the similar $T_{1/2}$ values and lack of abrupt transitions and thermal hysteresis suggest that incorporation into a polymeric, covalently linked species does not increase the communication between spin crossover centres. Further detailed structural comparisons of the materials are discussed below.

The dinuclear compounds **3a**, **3b**, **4a**, **4b**, **4c** and **4d** contain iron(II) and cobalt(II) coordination environments that involve Cl^- and H_2O groups and are thus expected to be HS-HS. Some interesting magnetic results were reported, however, for dinuclear systems by Gamez et al.[1] For example, [Fe(tdt)(NCCH$_3$)(H$_2$O)]$_2$(ClO$_4$)$_4$ displayed a gradual, partial spin crossover with a $T_{1/2}$ of ca. 280 K. This is unusual for iron(II) [FeN$_5$O] coordination environments. The replacement of acetonitrile by H_2O by exposure to air led to HS-HS magnetic behaviour, as expected, and similar to that noted for [Fe(tdt)(H$_2$O)(CH$_3$OH)]$_2$(BF$_4$)$_4$, also having [$Fe^{II}N_4O_2$] coordination.[1] A very small J value of –0.37 cm^{-1} was obtained for the latter, possibly with a zero-field splitting parameter of ca. 4 cm^{-1}, rather than J, being responsible for the rapid decrease in μ_{eff} being observed below 50 K.

Interestingly, the triazine *N*-bonded example [Fe(tdt)(Cl)]$_2$(CF$_3$SO$_3$)$_2$ was reported to show weak ferromagnetic coupling between the S = 2 Fe^{II} centres.[1] However, care has to be taken to exclude crystallite torquing effects as being the cause of increases in μ_{eff} in such $^5T_{2g}$ (parent) single-ion states and dispersal of the powder in Vaseline is the way to check for such effects. The magnetic behaviour of the present analogue [Fe(tdt)(Cl)]$_2$(ClO$_4$)$_2$·(C$_2$H$_5$OH)·2(CHCl$_3$) (**3a**) unfortunately could not be measured due to insufficient and impure amounts of bulk sample.

The cddt analogue [Fe(cddt)(NCCH$_3$)(H$_2$O)]$_2$(ClO$_4$)$_4$·(CH$_3$CN) (**4d**) contains the same iron(II) [FeN$_5$O] coordination environment as [Fe(tdt)(NCCH$_3$)(H$_2$O)]$_2$(ClO$_4$)$_4$ which, as discussed above, undergoes a gradual SCO. Here, the complex **4d** remains HS over all temperatures and the $\chi_M T$ vs. temperature plot is shown in Figure S12. The $\chi_M T$ values remain constant at 3.49 $cm^3 mol^{-1}$ K down to ca. 15 K, followed by a small decrease due to a combination of weak antiferromagnetic coupling and zero field splitting.

One-Dimensional Chain Complexes

General. [Fe(NCS)$_2$(cddt)]·n(guest) (1)

Crystal data and refinement details for the complexes **1a**, **1b** and **1c** can be found in Table 2. Three crystallographically distinct materials of the general formula [Fe(NCS)$_2$(cddt)]·*n*(guest) (**1**) have been synthesised and crystallised by slow diffusion techniques. All three phases are composed of one-dimensional (1D) chains which differ in their crystal packing and the number and type of solvent molecules. The general structures of **1a**, **1b** and **1c** are the same. However, as seen above, these three phases display vastly different magnetic properties [see part (a) of Figure 2 and Figure S11 in the Supporting Information]; **1a** and **1b** are HS and **1c**

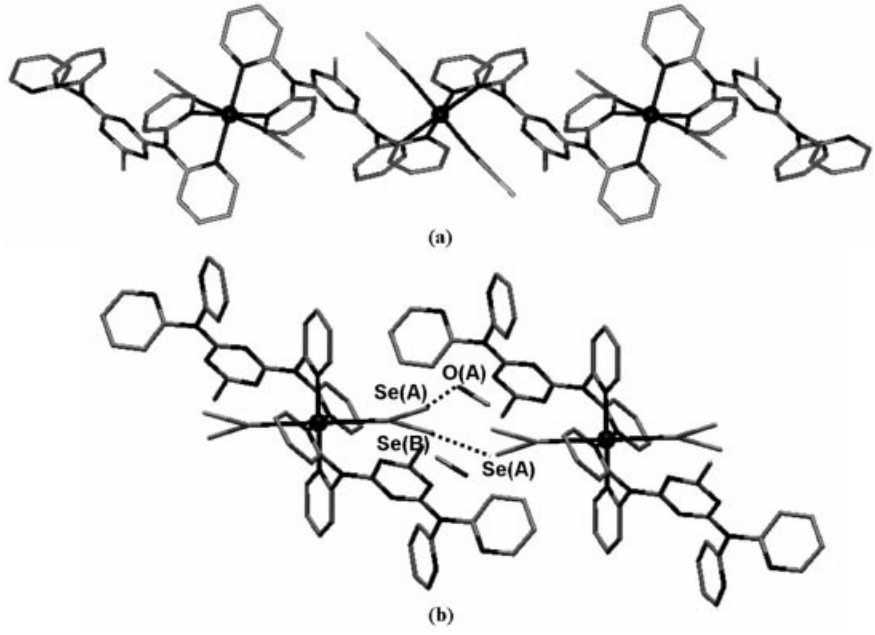

Figure 3. The general polymeric 1D chain structure observed in the materials (a) **1a**, **1b**, **1c** and (b) **2** illustrating the A and B positions of the disordered selenium atoms, the Se(A)···Se(B) interactions between adjacent chains and the Se(A)···O interactions are shown with dotted lines. Iron(II) centres are shown as black spheres, hydrogen atoms have been omitted.

undergoes a spin transition. The iron(II) environments and extended structure of these materials are, nevertheless, isostructural. These systems are highly relevant for making structural comparisons in order to attempt to determine both the intra- and inter-chain structural influence on the magnetism.

$[Fe(NCS)_2(cddt)]\cdot 1/2(CHCl_3)\cdot(H_2O)$ (**1a**) is grown as a pure crystalline phase by slow diffusion in methanol and chloroform. The two phases **1b** and **1c** are polymorphs, $[Fe(NCS)_2(cddt)]\cdot 2(CH_3OH)$, and grow simultaneously but they differ in their crystal symmetries (**1b**: monoclinic and **1c**: triclinic); **1c** is the major product. By subtle variation in the stoichiometry of reactants, **1c** can be grown in isolation, as indicated above. There have previously been in-depth studies into understanding the differences in spin crossover behaviours observed in polymorphic species;[20–24] here we will continue this, further, through detailed structural comparisons between each of the materials **1b** and **1c**.

All three phases, **1a**, **1b** and **1c** consist of iron(II) coordinated by *trans*-thiocyanate ligands bound through the terminal nitrogen and two half cddt ligands, the full ligands generated by symmetry [Figure 3 (a)]. The cddt ligands bridge two metal centres, binding via the terminal pyridyl groups of the bis(2-pyridyl)amine moiety. Each alternate ligand is rotated *ca*. 180° such that the triazine chlorine atom is directed up or down. This extends to form infinite 1D chains. Following are detailed structural descriptions of each of the three phases of **1**. The octahedral distortion parameter Σ has been calculated for each of the materials **1a**, **1b** and **1c**, smaller Σ values are associated with stronger crystal fields and stabilisation of the LS state.[27]

[Fe(NCS)$_2$(cddt)]·1/2(CHCl$_3$)·(H$_2$O) (1a)

Structural analysis of **1a** revealed a tetragonal symmetry with all iron(II) centres equivalent and with Fe–N distances typical of the HS iron(II) state (Table 1). The 1D chains are stacked parallel and run along the *c*-axis [Figure 4 (a)]. In the *ac*- and *bc*-planes the adjacent 1D chains are rotated by 90° [Figure 5 (a)]. Located between the chains are two types of alternating 1D channels along the *c*-axis which account for 23.4% of the unit cell volume [Figure 4 (a)]. The first type of channel is lined by the chlorine atoms from the cddt ligand and is filled with chloroform molecules. The second type of channel is lined by aromatic ligand rings and is filled by a 1D chain of water molecules. Neither the water or chloroform molecules interact with the 1D chains. It was surprising that since this material was synhesised in a mixed solvent system consisting of methanol and chloroform, no

Table 1. Selected bond lengths for **1a**, **1b**, **1c** and **2** obtained at 123 K.

Bond [Å]	**1a**	**1b**	**1c**	**2**
Fe(1)–N(CS)	2.083(9)	2.082(9)	1.953(5)	1.969(5)
Fe(1)–N(py)	2.223(9)	2.232(7)	1.995(4)	2.007(4)
Fe(1)–N(py)	2.237(8)	2.216(7)	2.002(4)	2.011(4)
Fe(2)–N(CS)	–	2.108(8)	2.084(5)	1.933(5)
Fe(2)–N(py)	–	2.198(6)	2.203(4)	2.016(4)
Fe(2)–N(py)	–	2.201(7)	2.226(4)	2.017(4)

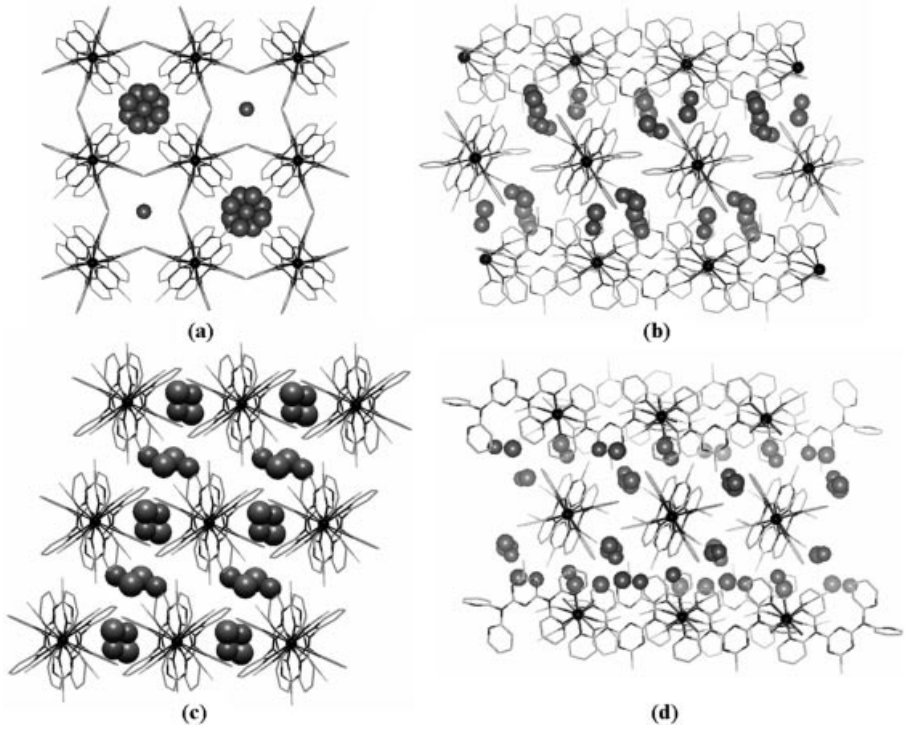

Figure 4. Illustration of the crystal packing of 1D chains and solvent in (a) **1a**, tetragonal, (b) **1b**, monoclinic, (c) **1c**, triclinic and (d) **2**, monoclinic. Hydrogen atoms have been omitted. Solvent molecules are represented by space-filling, iron(II) atoms as black spheres and 1D chains as sticks.

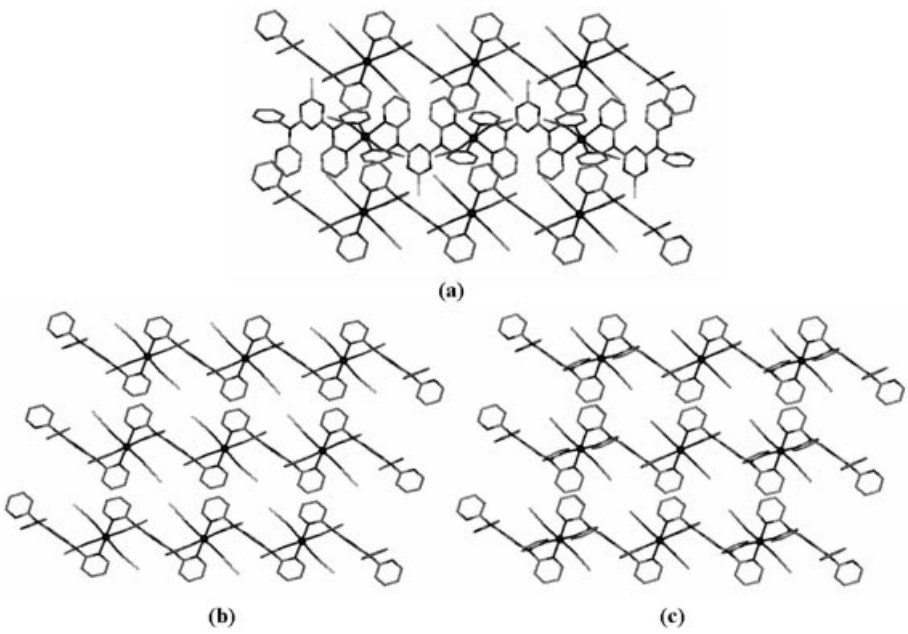

Figure 5. Illustration of the crystal packing of adjacent 1D chains in the *ab*-plane (a) **1a** (b) **1b** and (c) **1c**. Hydrogen atoms and solvent molecules have been omitted. Iron(II) atoms as black spheres and 1D chains as sticks.

methanol has been incorporated into the crystalline material. The chlorine atoms on the cddt ligand are involved in Cl···Cl interactions with adjacent chains [Cl···Cl: 3.204(10) Å]. Analysis of the geometry of the iron(II) centre revealed an octahedral distortion parameter Σ of 45.6° which is comparable to other $[Fe(N)_4(NCS)_2]$ centres in the HS state.[4,18,27] The Fe···Fe separation within each chain is 9.345(3) Å and this is similar to that between chains 9.258(2) Å.

[Fe(NCS)$_2$(cddt)]·2(CH$_3$OH) (1b)

The complex **1b** has different stacking of the 1D chains to that seen in both **1a** and **1c** [Figure 4 (b)]. Structural analysis of **1b** revealed a monoclinic symmetry with two iron(II) centres in the asymmetric unit which are both in the HS state at 123(2) K with average Fe–N bond lengths for Fe1 and Fe2 of 2.176(6) and 2.169(5) Å, respectively (Table 1). There are two crystallographically distinct thiocyanate ligands in the asymmetric unit; the sulfur atom of the thiocyanate ligand bound to Fe1 is disordered over two sites, **A** and **B** (Figure S2). The 1D chains are parallel packed in the *ab*-plane, where adjacent chains within the same *ab*-plane are generated by a translation along either the *a*- or *b*-axis [Figure 5 (b)]. The chains in the next *ab*-plane are rotated by 90° [Figure 4 (b)]. The Fe···Fe separation within each chain is 9.584(6) Å and smaller between chains, 8.717(6) Å. There are two solvent methanol molecules present in the asymmetric unit; one of the methanol molecules is hydrogen bonded to a sulfur atom of the **A** component of the disordered thiocyanate ligand [O2···S2A: 3.193(3) Å, Figure 5]. This thiocyanate ligand is also involved in a S···S interaction with its symmetry equivalent atom on an adjacent chain [S2A···S2A: 3.029(11) Å]. Neither the **B** component of the other thiocyanate ligand are involved in any significant O···S or S···S interactions. The most obvious distinction between the two iron(II) centres in the asymmetric unit is their hydrogen bonding interactions. However, further analysis of the metal centre geometries revealed that the iron(II) centre involved in the hydrogen bonding interaction, Fe1, is in a less distorted octahedral environment than is the other iron(II) centre, Fe2, thus, Σ(Fe1): 34.4 and Σ(Fe2): 44.8°.[27] The distortion parameter of Fe1 is considerably lower than Fe2 which is often indicative of the LS state being stabilised. However, while we do not have magnetic data, both iron(II) centres are in the HS state down to 123 K. The average Fe–N bond lengths for both Fe1 and Fe2 are indicative of high spin iron(II). Notably, the Fe2–N(CS) bond length is 2.108(8) Å, which is longer than the ca. 2.0 Å usually observed for iron(II). It is well known that weak intermolecular interactions can strongly influence the observed spin crossover features,[26] comparison of such features with **1c** will be discussed in the following section.

[Fe(NCS)$_2$(cddt)]·2(CH$_3$OH) (1c)

Structural analysis of **1c** at 123(2) K revealed a triclinic symmetry with two iron(II) centres in the asymmetric unit [Figure 4 (c)]. At 123(2) K, Fe1 is in the LS state and Fe2 is in the HS state with average Fe–N bond lengths of 1.983(3) and 2.171(4) Å, respectively (Table 1). This is a most unusual situation to have alternating HS and LS centres along the chains. In contrast, a recent iron(III) 1D system has been reported which contains isolated alternating HS and LS chains.[29]

The 1D chains in **1c** run along the *c*-axis, where adjacent chains are generated by a translation along either the *a*- or

b-axis as seen in **1b** [Figure 5 (c)]. In contrast to **1b**, all of the 1D polymer chains in **1c** run in the same direction, i.e., along the *c*-axis [Figure 4 (c)]. The Fe···Fe separation within each chain is 9.512(3) Å and between chains is 8.818(4) Å, which is similar to that observed for **1b**. There are two solvent methanol molecules present per metal centre and one of these molecules is hydrogen bonded to a sulfur atom of a thiocyanate [O2···S1: 3.267(5) Å]. In addition, there is a π-π interaction between a pyridyl ring coordinated to Fe1 and its symmetry generated ring on an adjacent chain, 3.699(2) Å. One of the pyridyl rings attached to Fe2 is also in the correct orientation for a π-π interaction with its symmetry equivalent however the distance of 4.699(2) Å is too long to be a significant interaction. It is well known that intramolecular π-π interactions influence spin transitions[28] and indeed the presence of such interactions in **1c**, but not in **1b**, is likely to determine whether spin crossover behaviour will be observed.

As discussed above, smaller octahedral distortion parameters generally suggest a more stabilised LS state.[27] Further analysis of the geometries of the two metal centres in **1c** revealed that the iron(II) centre involved in this hydrogen bonding interaction is in a less distorted octahedral environment than the other iron centre, Σ(Fe1): 32.28 and Σ(Fe2): 42.76° which has been observed previously for materials in an intermediate [HS-LS] state.[4,18,27] Interestingly, Σ is comparable for Fe1 and Fe2 in **1b** and **1c**, where only **1c** undergoes a spin transition. This suggests that the interplay between intermolecular interactions, as discussed above and metal coordination environments are influencing these systems greatly.

Variable-Temperature Powder X-ray Diffraction of 1c

Some difficulties were encountered in preparing phase pure bulk sample of **1c**, such as required for SQUID magnetometry, with up to ca. 10% impurity of **1b** typically observed. Consequently, it was necessary to confirm the nature of the (two-step) spin transition identified in this way. This was achieved using variable-temperature diffraction methods whereby the structural perturbations accompanying the changes in Fe–N bond length associated with the spin transition are evident as pronounced changes in the lattice dimensions. Typically a contraction in unit cell volume of 10% is observed for a full transition from high to low spin. While this approach can be applied to both single crystal[4,8,26] and powdered samples,[30] the latter probes bulk samples allowing the temperature dependence of lattice parameters of individual phases to be monitored and the component(s) undergoing structural transitions to be identified. Moreover, crystals of **1c** are typically twinned which would complicate single-crystal studies.

Here, variable temperature powder diffraction methods have been applied to study the structural and spin transition in **1c**. Powder diffraction data were collected at 3 K intervals upon cooling of the sample from 250 to 85 K, the temperature region in which the spin transition was observed. The lattice parameter of the majority phase was refined using a single phase Le Bail fit to the data (Figure S13) based on the crystal symmetry and lattice parameters determined in single crystal structural studies of **1c**.[40] The adequacy of the single phase refinement confirms the phase purity of the bulk sample used here.

The relative changes in the refined lattice parameters for **1c** upon cooling from 250 to 85 K are shown in Figure 6. Two sets of non-linear features evident in the temperature dependence of the lattice parameters for **1c** (at 250–200 K and ca. 125 K) support the two-step nature of the spin transition in this phase. The sharp contraction in the unit cell volume (ca. 2%) in the range 250–200 K correlates directly with the sharp decrease observed in the magnetic susceptibility at 250–200 K associated with a partial spin transition. This contraction was highly anisotropic, with different temperature dependent behaviour observed along the *a*-, *b*- and *c*-axes (Figure 6). A more gradual contraction in the unit cell volume (ca. 1.5%) occurs upon further cooling between 200 and 100 K, which corresponds to the second more gradual spin transition observed in the magnetic susceptibility. The magnitude of the volume contraction observed over the entire temperature range studied (ca. 3.5%), and those attributed to each step are consistent with the degree of spin transition indicated by the magnetic susceptibility measurements with a total volume contraction of 3–5% anticipated for this "half" spin-crossover phase. Although the intrinsic thermal expansion of the framework would also contribute to a contraction of the lattice with decreasing temperature, the non-linearity of the observed behaviour supports the existence of additional phenomena. This non-linearity is most evident for the individual cell axes. In particular, the *c*-axis, along which the 1D chains are oriented, is most directly sensitive to the spin transition and associated changes in the Fe–N bond length. This axis shows pronounced non-linear behaviour (a minimum) at ca.

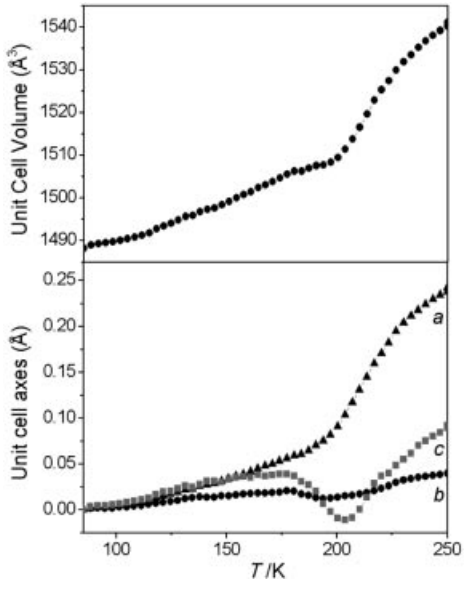

Figure 6. Unit cell volume (top) and axes (bottom) evolution vs. temperature for the spin transition in **1c** over the range 85–250 K obtained by synchrotron powder diffraction.

200 K and a more subtle non-linearity at ca. 125 K. Non-linear thermal expansion behaviour was also evident along the *a*- and *b*-axes which is associated with the contraction of Fe–N bonds oriented in the *ab*-plane, and structural perturbations which propagate via intermolecular interactions including the π-π interactions present in this phase.

[Fe(NCSe)$_2$(cddt)]·2(CH$_3$OH) (2)

Crystal data and refinement details of complex **2** can be found in Table 2. Structural analysis of **2** revealed a monoclinic symmetry, isomorphous to **1b**, with two iron(II) centres in the asymmetric unit. The selenocyanate sulfur atom attached to Fe2 is disordered over two crystallographically distinct sites, **A** and **B** (50:50 site occupancies). There is a Se···Se interaction between adjacent chains from the part **A** of the disordered selenocyanate to part **B** [Se···Se: 3.369(2), Figure 3 (b)]. The Se atoms associated with Fe1 are not involved in any interactions. There are two solvent molecules in the asymmetric unit, however one is only present 50% of the time and is associated with the **B** part of the disordered selenocyanate [Figure 3 (b)]. There are no π-π interactions present in this compound which is converse to the case in the thiocyanate analogue **1c**. The Fe···Fe separation within each chain is 9.330(2) Å and between chains is 8.988(2) Å, similar to that of **1b** and **1c**. Further analysis of the geometries of the two metal centres revealed octahedral distortion parameters for Fe1 and Fe2 of Σ: 30 and 26.04°, respectively.[27] Firstly, it can be seen that Fe1 is slightly more distorted than Fe2 in agreement with the presence of two crystallographically distinct metal centres in the asymmetric unit. Secondly, the distortion parameters for Fe1 and Fe2 are of the same magnitude and similar to the distortion parameter observed in **1c** for Fe1, i.e. 32.28°. Of great interest, here, is the large difference in octahedral distortion of the iron(II) centres between the isomorphous materials **1b** and **2**, which highlights the influence of the stronger ligand field of the $NCSe^-$ ligand. As discussed above, the π-π interactions observed in **1c** are thought to play a major role in influencing the spin transition, no such interactions are observed in **2**, however, the stronger ligand field strength of the $NCSe^-$ ligand compared to the NCS^- ligand would contribute towards the spin state of iron(II) and the observed crossover in **2**.

Dinuclear Fe^{II} and Co^{II} Complexes of tdt and cddt

General

Crystal data and refinement details for the dinuclear complexes **3a**, **3b**, **4a**, **4b**, **4c** and **4d** are summarised in Table 3. **3a** and **3b** contain the ligand tdt and their two kinds of dinuclear structures have been reported recently by Gamez et al.,[1] differing only in the anion and solvent present and so will not be discussed here in detail. **4a**, **4b**, **4c** and **4d** contain the ligand cddt and consist of isostructural dinuclear moieties that differ in their metals, associated anions and solvents.

[Fe(tdt)(Cl)]$_2$(ClO$_4$)$_2$·(C$_2$H$_5$OH)·2(CHCl$_3$) (3a)

The dinuclear complex **3a** consist of two iron(II) centres coordinated by two tdt ligand and two chloride ligands (Figure S5). The metal centres are in a distorted octahedral environment consisting of five Fe–N bonds from two tdt ligands, including a triazine N donor, and one terminal Fe–Cl bond. The average Fe–Cl and Fe–N bond lengths are 2.3386(18) and 2.2114(5) Å, respectively (Table S1), and correlated well with those of HS iron(II) and those reported by Gamez et al. for [Fe(tdt)(Cl)]$_2$·(CF_3SO_3).[1] The iron(II) centres are in an extremely distorted octahedral environment illustrated by the octahedral distortion parameters of 66.65°.[27] The Fe···Fe separation within the dinuclear moiety is 8.384(2) Å.

[Fe(tdt)(H$_2$O)$_2$]$_2$(ClO$_4$)$_4$·6(H$_2$O) (3b)

The dinuclear complex **3b** consists of two iron(II) centres coordinated by two tdt ligands and four terminal water molecules. The triazine nitrogen atoms do not coordinate. The average Fe–O and Fe–N bond lengths are 2.161(3) and 2.174(4) Å, respectively (Table S1), and correlated well with those of HS iron(II) and those reported by Gamez et al. for [Fe(tdt)(H_2O)(CH_3OH)]$_2$(BF_4)$_4$.[1] Here, however, we observed the coordination of two water molecules rather than one water and one methanol by Gamez et al.[1] The Fe···Fe separation within the dinuclear molecule is 9.215(2) Å.

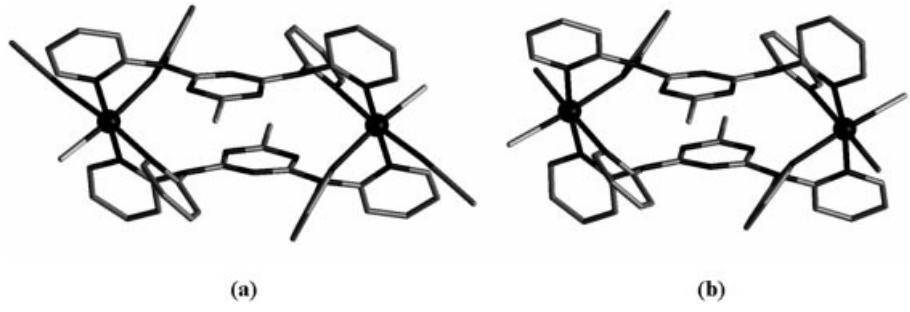

Figure 7. Structural representations of the dinuclear complexes containing the ligand cddt (a) **4a**, **4b**, **4c** and (b) **4d**.

[M(cddt)(H$_2$O)Cl]$_2$(X)$_2$·n(C$_2$H$_5$OH, H$_2$O) [M: Fe, X: ClO$_4$ (4a), M: Fe, X: BF$_4$ (4b), M: Co, X: BF$_4$ (4c)]

The dinuclear structures of **4a**, **4b** and **4c** generally consists of two metal(II) centres each in a distorted octahedral environment, two cddt ligands and terminal water and chlorine atoms [Figure 7 (a)]. Each cddt ligand is bound to two metal centres through both pyridyl groups of each di(pyrid-2-yl)amine, as seen in **3b**. The chlorine atoms of the cddt ligand are not involved in any interactions within the metal coordination sphere or any hydrogen bonding interactions. However, hydrogen bonding interactions are present between the metal coordinated chlorine atoms and the solvent water molecule [Cl···O: 3.149(4) (**4a**), 3.150(6) (**4b**) and F···O: 3.331(13) Å (**4c**)] and between the metal coordinated water molecules and the solvent ethanol [O···O: 2.703(5) Å (**4a**), 2.688(7) (**4b**) and 2.704(9) Å (**4c**)]. The Fe–N or Co–N bond lengths for each of these compounds are indicative of HS iron(II) or cobalt(II) (Table S1). The average Fe–Cl, Fe–O and Fe–N bond lengths for **4a** are 2.3954(13), 2.174(3) and 2.207(4) Å, respectively. The average Fe–Cl, Fe–O and Fe–N bond lengths for **4b** are 2.389(2), 2.164(5) and 2.206(5) Å, respectively. The average Co–Cl, Co–O and Co–N bond lengths for **4c** are 2.400(2), 2.136(5) and 2.160(6) Å, respectively. The Fe···Fe separations for **4a**, **4b** and **4c** within the dinuclears are 9.479(7), 9.459(9) and 9.351(5) Å, respectively.

[Fe(cddt)(NCCH$_3$)(H$_2$O)]$_2$(ClO$_4$)$_4$·(CH$_3$CN) (4d)

The general structure of **4d** is a dinuclear complex that is isostructural to **4a**, **4b** and **4c**, however, the coordinated chloride atoms are replaced here by acetonitrile molecules bound through the terminal nitrogen [Figure 7 (b)]. **4d** crystallises in the monoclinic space group $P2_1/n$ whereas **4a**, **4b** and **4c** crystallise in the monoclinic space group $C2/c$ (Table 3), resulting in a different packing of the dinuclear units within their respective unit cells. The average Fe–O and Fe–N bond lengths are 2.123(2) and 2.173(2) Å, respectively, and are indicative of HS iron(II) (Table S1). This same coordination environment was observed for the dinuclear complex [Fe(tdt)(NCCH$_3$)(H$_2$O)]$_2$(BF$_4$)$_4$·(CH$_3$CN) reported by Gamez et al.[1] and was observed to undergo a one step spin transition. Here the Fe–N and Fe–O bond lengths are comparable, but we observed no spin crossover. The Fe···Fe separation within the dinuclear is 9.068(2) Å, this distance is shorter both to that observed in **4a** and **4b** and in [Fe(tdt)(NCCH$_3$)(H$_2$O)]$_2$(BF$_4$)$_4$·(CH$_3$CN).[1]

Conclusions

Structural and magnetic studies of a range of polynuclear compounds using the dipyrid-2-ylamine containing ligands tdt and cddt have been carried out on a series of 1D polymers of the type [Fe(NCS)$_2$(cddt)$_2$]·*n*(guest) (**1a**, **1b**, and **1c**) and [Fe(NCSe)$_2$(cddt)$_2$]·*n*(guest) (**2**). A combination of such measurements has revealed the role of crystal packing and symmetry on the observed magnetic properties. Three crystal phases of **1** were obtained and exist in tetragonal (**1a**), monoclinic (**1b**) and triclinic (**1c**) symmetries, with only the triclinic phase displaying a thermally induced spin transition. Full structural comparisons of **1a**, **1b**, **1c** and **2** revealed very similar iron(II) coordination environments and extended 1D chain structures. Each of the compounds **1a**, **1b**, **1c** and **2** contain S···S or Se···Se interactions and solvent···S or Se hydrogen bonds, respectively. However, **1c** contains additional π-π interactions which are thought to be the major influence on the observed spin transition. The complex **2** does not contain any π-π interactions but undergoes a spin transition that is probably due to the increase ligand field strength of the NCSe$^-$ ligand compared to the NCS$^-$ ligand in **1c**.

1c displays a one-step half spin crossover with a slight two-step character at low temperatures. To differentiate between the presence of a second step or the possibility of sample impurity (due the possibly presence of three crystal phases), further structural characterisation was carried out by monitoring the unit cell evolution of **1c** at temperatures over the spin transition. All the crystals of **1c** grow twinned, hence single crystal techniques for this experiment were not viable so powder diffraction using synchrotron radiation was utilised. This technique has scope to be used, in future, to desolvate and resolvated powder samples, in situ, and monitor such influences on any spin transition observed.

The most celebrated iron(II) SCO chains are the triply-bridged 1,2,4-triazole complexes of type [Fe(4-R-1,2-triazole)$_3$](anion)$_2$.[31] These materials display abrupt spin transitions near to room temperature, with wide hysteresis widths, the $T_{1/2}$ and ΔT values varying with R and anion. No crystal structures have been obtained but they are assumed similar to the structurally characterised Cu^{II} 1D species.[32] They would possibly benefit from synchrotron powder XRD measurements of the kind given in Figure 6 to ascertain their phase purity and to see if hysteresis occurred in the structural data. In comparison to the present 1D compounds [Fe(NCS)$_2$(cddt)$_2$]·*n*(guest), **1c** and [Fe(NCSe)$_2$(cddt)$_2$]·*n*(guest), **2**, the tris-triazole complexes form more rigid *facially* bridging motifs, with Fe···Fe separations less than in the cddt systems. On this basis, it would appear that such rigidity would favour the strong cooperativity noted, compared to the weak cooperativity observed here in the more flexibly-bridged cddt species. This still begs the question of how, as the HS to LS transition occurs, all the Fe^{II} centres along the tris-μ-triazole chains are able to structurally adjust to accommodate the smaller coordination spheres existing in the LS state, be it in "an all at once" or a sequential process. Such readjustment should be more facile in the present systems. The inter-chain effects upon the Fe^{II} sites, modulated by anions or solvate molecules are, of course, very difficult to define.

Two dinuclear materials containing the ligand tdt have been structurally characterised that are isostructural to those recently reported by Gamez et al.[1] but with different counter anions and solvent molecules. Complex **3a** involves triazine N–Fe coordination, while complex **3b** does not. A similar series of dinuclear materials **4a**, **4b**, **4c** and **4d** containing the ligand cddt, of the **3b** structure type, have been

structurally characterised and shown to contain the same general dinuclear structure but differ in their counter anions and solvent molecules. Each of the dinuclear compounds containing either tdt or cddt ligands were intended to have both a FeN_6 coordination sphere through incorporation of the *N*-donor ligand thiocyanate, and display spin transitions. However, even though such a situation is sterically possible it is apparent that coordination of chloride atoms and/or water molecules is much more favourable. In the paper by Gamez et al.[1] it was suggested that extended framework materials incorporating the ligand tdt were possible, however all attempts, here, to synthesise such materials, using NCS^- as co-ligand, have resulted in the formation of the mononuclear spin crossover complex $Fe(NCS)_2(tdt)_2$ already reported.[2] The present direct synthesis contrasts with the report that it could only be made from dinuclear precursors.[2]

There are some interesting similarities and differences noted between the present dinuclear iron(II) compounds and the analogues described by Gamez et al.[1] If the effects of intermoleculear interactions in crystals are ignored, and the ligand-field around each iron(II) is assumed dominant, then the following conclusions can be made about the ligand-field and the spin state on the iron(II) centres. The complexes possessing a triazine N-donor $[Fe(tdt)(Cl)]_2(ClO_4)_2{\cdot}(C_2H_5OH){\cdot}2(CHCl_3)$ (**3a**) here, and the complex $[Fe(tdt)(Cl)]_2(CF_3SO_3)_2$ in Gamez et al.,[1] have a $[FeN_5Cl]$ coordination set and are both HS-HS. The other dinuclear type, not displaying triazine coordination are $[Fe(cddt)(NCCH_3)(H_2O)]_2(ClO_4)_4{\cdot}(CH_3CN)$ (**4d**) and the complex $[Fe(tdt)(NCCH_3)(H_2O)]_2(ClO_4)_4$ in Gamez et al.,[1] both with $[Fe_5NO]$ coordination. The SCO behaviours observed in the tdt system contrasts with the HS-HS behaviour in **4d** and, thus, tdt provides a stronger ligand-field contribution than does cddt.

Experimental Section

General: All the reagents and solvents were used as commercially available and used as received. The ligands tdt and cddt were prepared by literature methods.[33] Infrared spectra were recorded on single crystals mounted on a Low-e microscope slide using a Varian FTS7000 FT-IR spectrometer with a VMA600 microscope in reflectance mode. CHN analyses were performed by Campbell Microanalytical Laboratory, Department of Chemistry, University of Otago, Dunedin, New Zealand.

Magnetic Susceptibility Measurements: Magnetic susceptibility data were collected using a Quantum Design MPMS 5 SQUID magnetometer under an applied field of 1 T. The powder samples were placed in a quartz tube and great care was taken to avoid any solvent loss and/or torquing of crystallites of these potentially anisotropic HS iron(II) species, the latter by dispersal of the powder in a Vaseline mull. Care was also taken to allow long thermal equilibration times at each temperature point.

Crystallographic Data Collection and Refinement (Tables 2 and 3): Crystallographic data and parameters for all materials are summarised in Tables 2 and 3. Single crystal diffraction data for all structures were collected on a Bruker APEX X8 diffractometer using Mo-K_α (λ = 0.71073 Å) radiation and equipped with an Oxford Instruments nitrogen gas cryostream. Crystals were mounted on a MiTeGen MicroMounts fibre in a small amount of oil. Crystals were quench-cooled to 123(2) K for all data sets.

Diffraction data analysis was performed using SAINT+ within the APEX2 software package.[34] Empirical absorption corrections were applied to all data using SADABS.[35] The structures were solved using SHELXS and refined using SHELXL-97 within WINGX.[34,36] All non–hydrogen atoms in the structures were refined anisotropically and hydrogen atoms were generated using the riding model. The data set for the material **1c** was merohedrally twinned over two orientations related by a 179.9° rotation about the reciprocal axis 010. Initial indexing for the two components was carried out using CELL NOW within the APEX2 software package.[34] Multi-component integration was carried out using SAINT+.[34] Scaling and empirical absorption corrections were then applied using TWINABS.[34] The structure was solved as above using a HKLF 5 command with a resulting BASF parameter of 0.3477.

CCDC-625487 to -625496 contain the supplementary crystallographic data for this paper. These data can be obtained free of charge from The Cambridge Crystallographic Data Centre via www.ccdc.cam.ac.uk/datarequest/cif.

Table 2. Crystal data and refinement details for compounds **1a**, **1b**, **1c** and **2**.

	1a	**1b**	**1c**	**2**
Spin states	HS	HS	HS-LS	LS
T [K]	123(2)	123(2)	123(2)	123(2)
Empirical formula	$C_{51}H_{32}Cl_5Fe_2N_{22}O_2S_4$	$C_{27}H_{24}ClFeN_{11}O_2S_2$	$C_{27}H_{24}ClFeN_{11}O_2S_2$	$C_{27}H_{24}ClFeN_{11}O_2Se_2$
Formula mass/g mol^{-1}	1402.22	689.99	689.99	767.77
Crystal system (space group)	tetragonal (*P4/ncc*)	monoclinic ($P2_1/n$)	triclinic ($P\bar{1}$)	monoclinic ($P2_1/n$)
Z	4	4	2	2
a/Å	18.5157(6)	14.6590(4)	8.8106(5)	14.0888(7)
b/Å	18.5157(6)	12.3486(4)	9.4825(5)	12.2342(6)
c/Å	18.7076(10)	17.4349(6)	19.0242(11)	17.9765(9)
α/°	90.00	90.00	78.458(5)	90.00
β/°	90.00	102.0530(10)	77.652(3)	100.798(3)
γ/°	90.00	90.00	73.638(4)	90.00
V/Å^3	6413.5(5)	3086.46(17)	1473.08(14)	3043.7(3)
$\rho_{calcd.}$/Mg·m^{-3}	1.452	1.485	1.556	1.676
μ/mm^{-1}	0.848	0.757	0.793	3.019
$R(F)$/% [$I > 2\sigma(I)$, all]	0.1156 [0.1887]	0.0785 [0.0966]	0.0860 [0.0916]	0.0616 [0.1082]
$R_w(F^2)$/% [$I > 2\sigma(I)$, all]	0.3251 [0.3972]	0.2007 [0.2162]	0.1903 [0.1934]	0.1257 [0.1426]
GoF	1.009	1.050	1.210	1.034

Table 3. Crystal data and refinement details for compounds **3a**, **3b**, **4a**, **4b**, **4c** and **4d**.

	3a	**3b**	**4a**
T [K]	123(2)	123(2)	123(2)
Empirical formula	$C_{70}H_{56}Cl_{10}Fe_2N_{24}O_9$	$C_{66}H_{48}Cl_4Fe_2N_{24}O_{26}$	$C_{50}H_{46}Cl_6Fe_2N_{18}O_{13}$
Formula mass/g mol^{-1}	1843.59	1846.78	1431.45
Crystal system (space group)	triclinic ($P\bar{1}$)	monoclinic ($P2_1/n$)	monoclinic ($C2/c$)
Z	1	2	4
a/Å	12.9071(9)	13.430(3)	19.4533(3)
b/Å	13.1087(17)	14.303(3)	16.1016(2)
c/Å	13.2276(10)	20.390(4)	20.3064(3)
α/°	104.345(4)	90.00	90.00
β/°	115.873(2)	101.11(3)	110.6570(10)
γ/°	95.102(4)	90.00	90.00
V/Å^3	1900.4(3)	3843.2(13)	5951.63(15)
$\rho_{calcd.}$/Mg·m^{-3}	1.611	1.596	1.598
μ/mm^{-1}	0.808	0.614	0.835
$R(F)$/% [$I > 2\sigma(I)$, all]	0.1069 [0.1661]	0.0642 [0.1493]	0.0670 [0.1101]
$R_w(F^2)$/% [$I > 2\sigma(I)$, all]	0.2601 [0.3043]	0.1695 [0.2413]	0.1825 [0.2325]
GoF	1.062	1.063	1.158
	4b	**4c**	**4d**
T [K]	123(2)	123(2)	123(2)
Empirical formula	$C_{50}H_{46}B_2Cl_4F_8Fe_2N_{18}O_6$	$C_{50}H_{46}B_2Cl_4Co_2F_8N_{18}O_6$	$C_{52}H_{42}Cl_6Fe_2N_{21}O_{18}$
Formula mass/g mol^{-1}	1422.17	1428.33	1573.47
Crystal system (space group)	monoclinic ($C2/c$)	monoclinic ($C2/c$)	monoclinic ($P2_1/n$)
Z	4	4	2
a/Å	19.466(4)	19.4162(3)	12.6006(3)
b/Å	16.055(3)	15.9960(3)	14.6048(4)
c/Å	20.511(4)	20.4328(4)	18.1261(5)
α/°	90.00	90.00	90.00
β/°	112.24(3)	112.550(5)	106.6940(10)
γ/°	90.00	90.00	90.00
V/Å^3	5934(2)	5860.9(3)	3195.14(15)
$\rho_{calcd.}$/Mg·m^{-3}	1.592	1.619	1.635
μ/mm^{-1}	0.760	0.840	0.793
$R(F)$/% [$I > 2\sigma(I)$, all]	0.0790 [0.1799]	0.0979 [0.2111]	0.0577 [0.0626]
$R_w(F^2)$/% [$I > 2\sigma(I)$, all]	0.2000 [0.2968]	0.2198 [0.3061]	0.1395 [0.1424]
GoF	0.998	1.122	1.085

Powder Synchrotron X-ray Diffraction: A pulverised sample of $[Fe(NCS)_2(cddt)]\cdot 2(CH_3OH)$ (**1c**) was loaded in a polyimide capillary of 0.8 mm diameter and kept in an inert helium atmosphere for the duration of the experiments.[37] The X-rays (20.02 keV, 0.61915 Å) available at the 1-BM beamline at the Advanced Photon Source at Argonne National Laboratory were used in combination with a MAR-345 imaging plate (IP) detector to record diffraction patterns. The sample temperature was controlled using an Oxford Cryosystems Cryostream 700 and data were collected in 1 s exposures upon continuous cooling from 250 K to 85 K at 100 Kh^{-1}. This corresponds to the collection of diffraction images at 3 K intervals. The raw images were processed using Fit-2D.[38–39] The sample-to-detector distance and tilt of the IP relative to the beam were refined using a LaB_6 standard. Le Bail analyses of the variable-temperature diffraction data were performed within GSAS.[40] Details of the refinements are included in the Supporting Information.

$[Fe(cddt)(NCS)_2]\cdot 1/2(CHCl_3)\cdot(H_2O)$ (1a): A 5 mL solution of cddt (45 mg, 0.1 mmol) in chloroform was placed at the base of a test tube onto which an 8 mL 50:50 mixture of methanol/chloroform was carefully layered. A 5 mL solution of $Fe(ClO_4)_2\cdot 6(H_2O)$ (25 mg, 0.1 mmol) and NaNCS (16 mg, 0.2 mmol) in methanol was then layered on-top and the test tube stoppered. After two weeks bright yellow needle shaped crystals formed (61 mg, 88%). IR: ν = 3445 (br), 2062 (s), 1604 (m), 1554 (m), 1466 (s), 1261 (m), 658 (w). $C_{51}H_{32}Cl_5Fe_2N_{22}O_2S_4$ (1402): calcd. C 39.97, H 2.71, N 19.72; found C 39.69, H 3.15, N 17.85.

$[Fe(cddt)(NCS)_2]\cdot 2(CH_3OH)$ (1b): A 2 mL solution of cddt (22 mg, 0.05 mmol) in methanol was placed at the base of one arm of an H-shaped tube. A 2 mL solution of $Fe(ClO_4)_2\cdot 6(H_2O)$ (25 mg, 0.1 mmol) and NaNCS (16 mg, 0.2 mmol) was placed in the other arm of the H-shaped tube. Solvent methanol was carefully layered to fill the tube, which was then stoppered. After one week yellow block shaped crystals formed (yield: unknown forms as a mixed product with **1c** ca. 10%). IR: ν = 3440 (br), 2063 (s), 1598 (m), 1550 (m), 1465 (m), 1264 (m), 668 (w).

$[Fe(cddt)(NCS)_2]\cdot 2(CH_3OH)$ (1c): A 2 mL solution of cddt (45 mg, 0.1 mmol) in methanol was placed at the base of one arm of an H-shaped tube. A 2 mL solution of $Fe(ClO_4)_2\cdot 6(H_2O)$ (25 mg, 0.1 mmol) and NaNCS (16 mg, 0.2 mmol) was placed in the other arm of the H-shaped tube. Solvent methanol was carefully layered to fill the rest of the tube, which was then stoppered. After one week yellow block shaped crystals formed (60 mg, 87%). IR: ν = 3440 (br), 2057 (s), 1603 (m), 1552 (m), 1399 (s), 1229 (m), 670 (w). $C_{27}H_{24}ClFeN_{11}O_2S_2$ (689): calcd. C 47.9, H 2.58, N 24.62; found C 47.6 H 2.73, N 24.48.

$[Fe(cddt)(NCSe)_2]\cdot 2(CH_3OH)$ (2): A 5 mL solution of cddt (45 mg, 0.1 mmol) in methanol was placed at the base of one arm of an H-tube. A 2 mL solution of $Fe(ClO_4)_2\cdot 6(H_2O)$ (25 mg, 0.1 mmol) and

KNCSe (28 mg, 0.2 mmol) in methanol was placed in the other arm of the H-shaped tube. Solvent methanol was carefully layered to fill the rest of the H-tube, which was then stoppered. After two weeks bright yellow needle shaped crystals formed (58 mg, 74%). IR: ν = 3400 (br), 2061 (s), 1603 (m), 1552 (m), 1398 (m), 1230 (m), 656 (m). $C_{27}H_{24}ClFeN_{11}O_2Se_2$ (768): calcd. C 41.72, H 2.24, N 21.41; found C 43.70 H 2.93 N 21.54.

$[Fe(tdt)(Cl)]_2(ClO_4)_2\cdot(C_2H_5OH)\cdot2(CHCl_3)$ (3a): A 2 mL solution of tdt (59 mg, 0.1 mmol) in chloroform was placed at the base of one arm of an H-shaped tube. A 2 mL solution of $Fe(ClO_4)_2\cdot6(H_2O)$ (25 mg, 0.1 mmol) and $NaNCBH_3$ (12 mg, 0.2 mmol) in ethanol was placed in the other arm of the H-shaped tube. Solvent ethanol was carefully layered to fill the rest of the H-tube, which was then stoppered. After two weeks yellow block shaped crystals formed (120 mg, 32%). IR: ν = 3385 (br), 1601 (w), 1547 (m), 1466 (m), 1368 (s), 1008 (br). $C_{70}H_{56}Cl_{10}Fe_2N_{24}O_9$ (1843): calcd. C 40.93, H 3.64, N 16.84; found C 39.93, H 3.08, N 18.67.

$[Fe(tdt)(H_2O)]_2(ClO_4)_4\cdot6(H_2O)$ (3b): A 2 mL solution of tdt (59 mg, 0.1 mmol) in methanol and a 2 mL solution of $Fe(ClO_4)_2\cdot6H_2O$ (25 mg, 0.1 mmol) in acetonitrile were mixed in a vial. Over a period of 2 weeks yellow block crystals formed (125 mg, 36%). IR: ν = 3386 (br), 1602 (w), 1547 (m), 1466 (m), 1368 (s), 1001 (br). $C_{66}H_{48}Cl_4Fe_2N_{24}O_{26}$ (1743): calcd. C 41.68, H 3.39, N 17.68; found C 42.53, H 3.78, N 17.75.

$[Fe(cddt)(H_2O)Cl]_2(ClO_4)_2\cdot2(C_2H_5OH)\cdot(H_2O)$ (4a): A 2 mL solution of cddt (45 mg, 0.1 mmol) in ethanol and a 2 mL solution of $Fe(ClO_4)_2\cdot6H_2O$ (25 mg, 0.1 mmol) in ethanol were mixed in a vial. Over a period of 2 weeks yellow block crystals formed (150 mg, 52%). IR: ν = 3198 (br), 1601 (m), 1548 (m), 1466 (m), 1371 (s), 1050 (br). $C_{50}H_{46}Cl_6Fe_2N_{18}O_{13}$ (1431): calcd. C 36.27, H 3.84, N 16.55; found C 35.97, H 3.84, N 16.55.

$[Fe(cddt)(H_2O)Cl]_2(BF_4)_2\cdot2(C_2H_5OH)\cdot2(H_2O)$ (4b): A 2 mL solution of cddt (45 mg, 0.1 mmol) in ethanol and a 2 mL solution of $Fe(BF_4)_2\cdot6H_2O$ (34 mg, 0.1 mmol) in acetonitrile were mixed in a vial. Over a period of 2 weeks yellow block crystals formed (160 mg, 56%). IR: ν = 3199 (br), 1601 (m), 1548 (m), 1465 (m) 1368 (s), 1052 (br).

$[Co(cddt)(H_2O)Cl]_2(BF_4)_2\cdot2(C_2H_5OH)\cdot2(H_2O)$ (4c): A 2 mL solution of cddt (45 mg, 0.1 mmol) in ethanol and a 2 mL solution of $Co(BF_4)_2\cdot6H_2O$ (34 mg, 0.1 mmol) in acetonitrile were mixed in a vial. Over a period of 2 weeks orange block crystals formed (175 mg, 61%). IR: ν = 3358 (br), 1602 (m), 1546 (m), 1467 (m), 1371 (s), 1053 (br). $C_{50}H_{46}B_2Cl_4Co_2F_8N_{18}O_6$ (1428): calcd. C 43.34, H 3.64, N 17.84; found C 44.55, H 3.89, N 18.78.

$[Fe(cddt)(NCCH_3)(H_2O)]_2(ClO_4)_4\cdot(CH_3CN)$ (4d): A 2 mL solution of cddt (45 mg, 0.1 mmol) in acetonitrile was placed at the base of one arm of an H-shaped tube. A 2 mL solution of $Fe(ClO_4)_2$ (25 mg, 0.1 mmol) in acetonitrile was placed in the other arm of the H-shaped tube. Neat acetonitrile was carefully layered to fill the rest of the H-tube, which was then stoppered. After two weeks yellow block shaped crystals formed. (200 mg, 63%). IR: ν = 2130 (w), 2138 (w), 1607 (m), 1550 (m), 1387 (s), 1260 (w), 1229 (w), 1118 (br), 623 (m). $C_{52}H_{42}Cl_6Fe_2N_{21}O_{18}$ (1573): calcd. C 39.62, H 2.88, N 18.04; found C 39.13, H 3.02, N 18.04.

Supporting Information (see also the footnote on the first page of this article): Thermal ellipsoid diagrams, including numbering schemes for all materials discussed here are included. Table of selected bond lengths of the dinuclear materials are included. Additional magnetic susceptibility plots for selected materials are also included. Detailed refinement and processing of powder diffraction data, including tables of χ^2 values.

Acknowledgments

This work was supported by an ARC Discovery Grant (KSM) and the Australian Synchrotron Research Program, which is funded by the Commonwealth of Australia under the Major National Research Facilities Program. Use of the Advanced Photon Source was supported by the U.S. Department of Energy, Office of Science, Basic Energy Sciences, under Contract No. DE-AC02-06CH11357.

[1] M. Quesada, P. de Hoog, P. Gamez, O. Roubeau, G. Aromí, B. Donnadieu, C. Massera, M. Lutz, A. L. Spek, J. Reedijk, *Eur. J. Inorg. Chem.* **2006**, *7*, 1353–1361.
[2] M. Quesada, M. Monrabal, G. Aromí, V. de la Peña-O'Shea, M. Gich, E. Molins, O. Roubeau, S. Teat, E. MacLean, P. Gamez, J. Reedijk, *J. Mater. Chem.* **2006**, *26*, 2669–2676.
[3] B. A. Leita, B. Moubaraki, K. S. Murray, J. P. Smith, J. D. Cashion, *Chem. Commun.* **2004**, 156–157.
[4] J. J. M. Amoore, C. J. Kepert, J. D. Cashion, B. Moubaraki, S. M. Neville, K. S. Murray, *Chem. Eur. J.* **2006**, *12*, 8220–8227.
[5] C. Schneider, J. D. Cashion, B. Moubaraki, S. M. Neville, S. R. Batten, D. R. Turner, K. S. Murray, *Polyhedron* **2006**, doi:10.1016/j.poly.2006.09.003.
[6] K. Nakano, S. Kawata, K. Yoneda, A. Fuyuhiro, T. Yagi, S. Nasu, S. Morimoto, S. Kaizaki, *Chem. Commun.* **2004**, *24*, 2892–2893.
[7] K. Yoneda, K. Nakano, J. Fujioka, K. Yamada, T. Suzuki, A. Fuyuhiro, S. Kawata, S. Kaizaki, *Polyhedron* **2005**, *24*, 2437–2442.
[8] G. J. Halder, C. J. Kepert, B. Moubaraki, K. S. Murray, J. D. Cashion, *Science* **2002**, *298*, 1762–1765.
[9] C. J. Kepert, *Chem. Commun.* **2006**, 695–700.
[10] S. M. Neville, B. Moubaraki, K. S. Murray and C. J. Kepert, *Angew. Chemie. Int. Ed.*, **2006**, submitted.
[11] O. Kahn, C. J. Martinez, *Science* **1998**, *279*, 44.
[12] J. A. Real, E. Andres, M. C. Muñoz, M. Julve, T. Granier, A. Bousseksou, F. Varret, *Science* **1995**, *268*, 265–267.
[13] V. Niel, A. L. Thompson, M. C. Muñoz, A. Galet, A. S. E. Goeta, J. A. Real, *Angew. Chem. Int. Ed.* **2003**, *42*, 3760–3763.
[14] K. Yoneda, K. Adachi, S. Hayami, Y. Maeda, M. Katada, A. Fuyuhiro, S. Kawata, S. Kaizaki, *Chem. Commun.* **2006**, *1*, 45–47.
[15] K. S. Murray, C. J. Kepert, *Top. Curr. Chem.* **2004**, *233*, 195.
[16] A. B. Gaspar, M. C. Muñoz, J. A. Real, *J. Mater. Chem.* **2006**, *16*, 2522–2533.
[17] S. R. Batten, J. Bjernemose, P. Jensen, B. A. Leita, K. S. Murray, B. Moubaraki, J. Smith, H. Toftlund, *Dalton Trans.* **2004**, 3370–3375.
[18] A. B. Gaspar, G. Agustí, V. Martínez, M. C. Muñoz, G. Levchenko, J. A. Real, *Inorg. Chim. Acta* **2005**, 4089–4094.
[19] Y. Garcia, O. Kahn, L. Rabardel, B. Chansou, L. Salmon, J. P. Tuchagues, *Inorg. Chem.* **1999**, *38*, 4663.
[20] A. Galet, M. C. Muñoz, A. B. Gaspar, J. A. Real, *Inorg. Chem.* **2005**, *44*, 8749–8755.
[21] A. Galet, M. C. Muñoz, V. Martínez, J. A. Real, *Chem. Commun.* **2004**, 2268–2269.
[22] E. König, K. Madeja, *Inorg. Chem.* **1967**, *6*, 48.
[23] E. König, K. Madeja, K. J. Watson, *J. Am. Chem. Soc.* **1968**, *90*, 1146.
[24] A. Ozarowski, B. R. McGarvey, A. B. Sarkar, J. E. Drake, *Inorg. Chem.* **1988**, *27*, 628.
[25] S. Matouzenko, A. Bousseksou, S. Lecoca, P. J. van Koningsbruggen, M. Perrin, O. Kahn, A. Kollet, *Inorg. Chem.* **1997**, *36*, 5869.
[26] M. Marchivie, P. Guionneau, J.-F. Letard, D. Chasseau, *Acta Crystallogr., Sect. B* **2003**, *59*, 479–486.

[27] P. Guionneau, C. Brigouleix, Y. Barrans, A. E. Goeta, J.-F. Létard, J. A. Howard, J. Gaultier, D. C. Chasseau, *R. Acad. Sci. Ser. IIc* **2001**, *4*, 161–171.
[28] P. Guionneau, M. Marchivie, G. Bravic, J.-F. Letard, D. Chasseau, *Top. Curr. Chem.* **2004**, *234*, 97–128.
[29] S. Imatomi, R. Kitashima, T. Hamamatsu, M. Okeda, Y. Ogawa, N. Matsumoto, *Chem. Lett.* **2006**, *35*, 502.
[30] K. W. Chapman, P. J. Chupas, C. J. Kepert, *J. Am. Chem. Soc.* **2006**, *128*, 7009–7014.
[31] Y. Garcia, V. Niel, C. Muñoz, J. A. Real, *Top. Curr. Chem.* **2004**, *233*, 229–257.
[32] A. Michalowicz, G. L. Moscovici, Y. Garcia, O. Kahn, *J. Synchrotron Radiat.* **1999**, *6*, 231.
[33] P. De Hoog, P. Gamez, W. L. Driessen, J. Reedijk, *Tetrahedron Lett.* **2002**, *43*, 6783.
[34] *APEX2 Software Package v 1.27*. Bruker AXS Inc., Madison, WI, **2005**.
[35] G. M Sheldrick, *SADABS, Empirical adsorption correction program for area detector data*, University of Göttingen, Germany, **1996**.
[36] L. J. Farugia, *J. Appl. Chem.* **1999**, *32*, 837–838.
[37] P. J. Chupas, M. F. Ciraolo, J. C. Hanson, C. P. Grey, *J. Am. Chem. Soc.* **2001**, *123*, 1694–1702.
[38] A. P. Hammersley, *ESRF Internal Report*, **1997**, ESRF97HA02T.
[39] A. P. Hammersley, S. O. Svensson, M. Hanfland, A. N. Fitch, D. Hausermann, *High-Pressure Res.* **1996**, *14*, 235–248.
[40] A. C. Larson, R. B. V. Dreele, *General Structure Analysis System (GSAS)*, **2000**, Los Alamos National Laboratory Report, LAUR 86–748.

Received: November 3, 2006
Published Online: January 25, 2007

